Spectroscopy of the proton drip-line nucleus ^{203}Fr

U. Jakobsson,[1,*] S. Juutinen,[1] J. Uusitalo,[1] M. Leino,[1] K. Auranen,[1] T. Enqvist,[2] P. T. Greenlees,[1] K. Hauschild,[3] P. Jones,[1,†] R. Julin,[1] S. Ketelhut,[1,‡] P. Kuusiniemi,[2] M. Nyman,[1,§] P. Peura,[1] P. Rahkila,[1] P. Ruotsalainen,[1] J. Sarén,[1] C. Scholey,[1] and J. Sorri[1]

[1]*Department of Physics, University of Jyväskylä, P.O. Box 35, FI-40014, Jyväskylä, Finland*

[2]*Oulu Southern Institute and Department of Physics, University of Oulu, Finland*

[3]*CSNSM, IN2P3-CNRS, F-91405 Orsay Campus, France*

(Received 21 January 2013; revised manuscript received 12 February 2013; published 17 May 2013)

The nucleus ^{203}Fr has been studied through γ-ray and electron spectroscopy, using the recoil-decay tagging technique. A $13/2^+$ state, with a half-life of 0.37(5) μs, has been observed in ^{203}Fr. Both the α-decay branch and the internal de-excitation of the $1/2^+$ isomer in ^{203}Fr have been studied. Furthermore, the corresponding $1/2^+$ state, with a half-life of 0.31(8) s, has been found in ^{199}At. In addition, transitions feeding the $9/2^-$ ground state of ^{203}Fr have been identified. The observed level pattern suggests that the ground state is still spherical.

DOI: 10.1103/PhysRevC.87.054320 PACS number(s): 23.20.Lv, 23.35.+g, 27.80.+w, 29.30.Kv

I. INTRODUCTION

Coexisting spherical, oblate and prolate shapes have been found to exist in neutron-deficient nuclei around lead up to $Z = 84$ (see Ref. [1] and references therein). The transition from spherical to deformed shapes, when approaching the neutron midshell, is believed to be caused by the increasing number of neutron holes coupled to the particle-hole excitations across the proton shell gap.

An onset of oblate ground-state deformation, associated with the 2p-2h excitation across the proton shell gap, has been reported to occur in even-mass polonium nuclei with $N \leqslant 114$ [2–4]. Low-lying excited states in neutron-deficient even-even radon nuclei have been studied down to ^{198}Rn [5–10]. An increase in collectivity for these states, caused by the increasing number of neutron-hole pairs has been observed, and contributions from the 2p-2h excitation have been suggested as well. α-decay properties obtained for ^{196}Rn [11] suggest an onset of oblate ground-state deformation in ^{196}Rn. The chain of neutron-deficient odd-mass francium nuclei is less well known than the radon isotopes, with ^{205}Fr being the lightest isotope with in-beam studies reported to date [12–15]. No onset of ground-state deformation has been observed in these nuclei, although we reported an increase of collectivity for the states feeding the ground state in ^{205}Fr [15].

Similarly to the 2p-2h excitation in even-even lead nuclei, the $1/2^+$ state, well known throughout the neutron-deficient odd-mass bismuth nuclei, is also associated with the intruder mechanism. The state comes down in energy with decreasing neutron number and becomes the ground state in ^{185}Bi [16]. Interesting features have been observed related to this state, such as very slow $M4$ transitions to the $9/2^-$ ground state [17]. In astatine nuclei the $1/2^+$ state is first observed in ^{197}At [18], decaying by α-particle emission, and becoming the ground state in ^{195}At [19]. Uusitalo *et al*. have previously observed the corresponding $1/2^+$ state in ^{203}Fr and ^{201}Fr through α-decay studies [20]. In ^{201}Fr the level lies at 146 keV, but in ^{203}Fr the level energy has not been established, as the corresponding state in the α-decay daughter ^{199}At has not yet been observed. The $1/2^+$ state, presumed to be oblate, is expected to become the ground state in ^{199}Fr [20].

Another state, characteristic of this region, is the $13/2^+$ state based on the odd proton excited to the $i_{13/2}$ orbital. Throughout the neutron-deficient odd-mass bismuth and astatine nuclei this state is better known than the $1/2^+$ state. For instance, when approaching the neutron midshell, the $13/2^+$ state becomes isomeric in ^{201}At [21], yrast in ^{199}At [22] and α decaying in ^{193}At [23]. In ^{199}At, ^{197}At [22], and ^{195}At [24] rotational bands, consistent with oblate deformation, have been observed to be built on top of the $13/2^+$ state. Among the odd-mass francium nuclei with $A < 213$, the $13/2^+$ state has so far only been observed in ^{205}Fr [15]. It is still non-yrast with a weakly deformed rotational band built on top of the isomer.

The present work investigates the possibility of shape coexistence in ^{203}Fr. Isomeric states involving the $\pi i_{13/2}$ and the $\pi s_{1/2}$ orbitals, respectively, are presented. An observation of the $1/2^+$ state in the α-decay daughter ^{199}At is reported as well. Prompt γ-ray transitions to the $9/2^-$ ground state have been observed and a level scheme for ^{203}Fr is presented. Additionally, a number of γ-ray transitions associated with the neighboring nucleus ^{204}Fr are presented.

II. EXPERIMENT

The experiment was performed at the Accelerator Laboratory at the Department of Physics of the University of Jyväskylä (JYFL), Finland. The ^{203}Fr nuclei were produced in the fusion-evaporation reaction ^{169}Tm(^{40}Ar, $6n$)^{203}Fr. The ^{40}Ar beam, provided by the K-130 cyclotron, was accelerated

*ulrika.jakobsson@jyu.fi

†Present address: iThemba Laboratory for Accelerator Based Sciences, P. O. Box 722, 7129 Somerset West, South Africa.

‡Present address: TRIUMF, Westbrook Mall, Vancouver, BC, V6T 2A3, Canada.

§Present address: European Commission, Joint Research Centre, Institute for Reference Materials and Measurements (IRMM), Retieseweg 111, B-2440 Geel, Belgium.

to an energy of 205 MeV with an average beam current of 13 particle-nA (pnA), during an irradiation time of 68 h in total. The self-supporting ^{169}Tm target had a thickness of 410 μg/cm^2. The ^{203}Fr nuclei were produced with a cross section of 4 μb.

The JUROGAM Ge-detector array was used to detect prompt γ rays at the target position. The array consisted of 43 Compton-suppressed high-purity germanium (HPGe) detectors of EUROGAM phase one [25] and GASP [26] type. The recoiling fusion-evaporation products were separated from beam particles and other unwanted reaction products by the gas-filled recoil separator RITU [27] and transported to the GREAT spectrometer [28] at its focal plane. When arriving in GREAT, the recoils passed through a multiwire proportional counter (MWPC) and were finally implanted into a 300-μm-thick double-sided silicon strip detector (DSSD), which has 4800 pixels in total. The horizontal strips of the DSSD were set to measure α-particle energies and the vertical strips to measure conversion-electron energies, by adjusting the gain ranges of the amplifiers. A clover germanium and a planar germanium detector close to the DSSD were used to detect delayed γ rays, and a silicon PIN-detector array, situated upstream in a box arrangement at the edges of the DSSD, was used for detecting conversion electrons. The PIN detectors and the vertical strips of the DSSD were calibrated using a ^{133}Ba source. All data channels were recorded synchronously using the triggerless total data readout (TDR) [29] data acquisition system, which gives each event an absolute time stamp with a time resolution of 10 ns.

III. RESULTS

The recoil-decay tagging (RDT) technique [30–32] was used in the experiment and the measurement data were processed using the GRAIN [33] and RADWARE [34,35] software packages. The recoiling fusion-evaporation products were selected by their time of flight between the MWPC and the DSSD and their energy loss in the MWPC. Furthermore, the different isotopes were identified by linking the recoils with their subsequent α decays in the DSSD, using spatial and temporal correlations. An α-decay branch close to 100% and a half-life of 0.55(1) s for the $9/2^-$ ground state [36] allowed for an effective identification of the ^{203}Fr recoils. A maximum correlation time of 1.5 s was used between the implantation of the recoil and its subsequent α decay. The energy spectrum of MWPC-vetoed α particles obtained from the ^{40}Ar + ^{169}Tm reaction is shown in Fig. 1. Conversion electrons and γ rays belonging to ^{203}Fr were identified based on their time correlation with the α-tagged recoil observed in the DSSD.

The energy spectra of delayed γ rays and electrons shown in Fig. 2 represent events detected with the GREAT clover detector and the PIN-detector array, respectively, tagged with the ^{203}Fr ground-state α decay. A peak with an energy of 426(1) keV is pronounced in the γ-ray spectrum. The two peaks in the electron spectrum represent the internal K- and $L + M + \ldots$-conversion peaks of this 426-keV γ-ray transition, respectively. The extracted $K/(L + M + \ldots)$ ratio of 3.3(4) indicates that the transition is of $M2$ character.

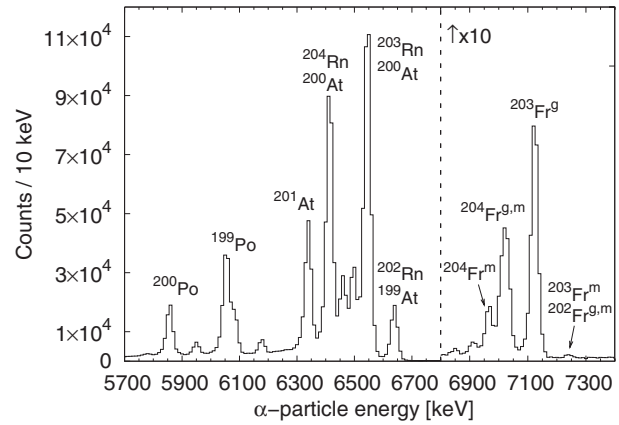

FIG. 1. Energy spectrum of MWPC-vetoed α particles obtained from the ^{40}Ar + ^{169}Tm reaction. For the α-particle energies of the francium nuclei, see, for example, Refs. [20,47].

The corresponding theoretical value is 3.1(3) as extracted from Ref. [37]. This value differs significantly from the corresponding values of 4.2(6) and 1.6(1) extracted for $M1$ and $E2$ transitions, respectively. By studying the time differences between the implantation of the ^{203}Fr recoil and the detection of the subsequent electrons (see inset of Fig. 2), a half-life of 0.37(5) μs was obtained, resulting in a transition strength of 0.10(2) W.u. for the $M2$ transition. The result is comparable with known values of $M2$ transitions depopulating the $13/2^+$ states directly to the $9/2^-$ ground states in neighboring odd-mass nuclei (for example 0.17(4) W.u. in ^{205}Fr [15], 0.182(22) W.u. in ^{201}At [38], 0.16(5) W.u. in ^{199}At [22], and 0.086(13) W.u. in ^{197}At [39]). Based on these observations the spin and parity of the isomer were assigned as $13/2^+$.

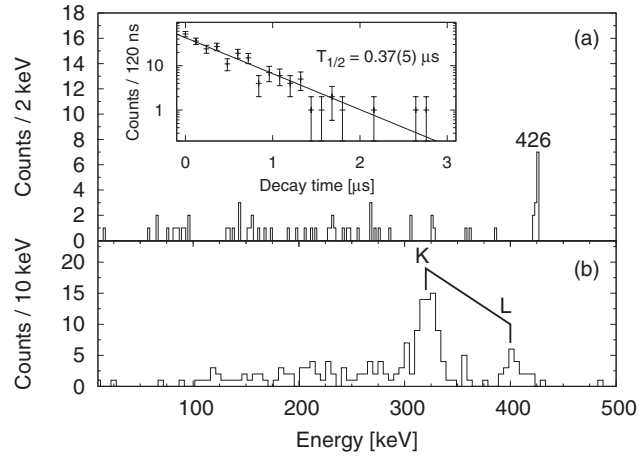

FIG. 2. Energy spectrum of delayed (a) γ rays detected with the GREAT clover detector and (b) conversion electrons detected with the GREAT PIN-detector array, tagged with the ^{203}Fr ground-state α decay. A maximum correlation time of 1.2 μs was set between the recoil implantation and the detection of an isomeric transition. The inset presents the distribution of time differences between the recoil implantation and the detection of the electron with the PIN-detector array. The half-life was obtained through a least squares fit to the data.

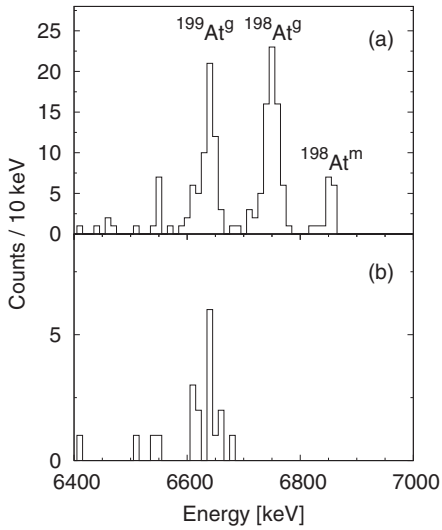

FIG. 3. (a) Energy spectrum of α particles from the decay of the daughter astatine nuclei following the α decay of the francium nuclei in Fig. 1 with the energy of ~7240 keV. (b) Energy spectrum of the α particles in (a) including the requirement of a conversion electron temporally between the two α decays in the same pixel of the DSSD. The ^{198}At events are filtered out. A maximum correlation time of 21 s has been used between the recoil implantation and the α decay of the daughter astatine nucleus.

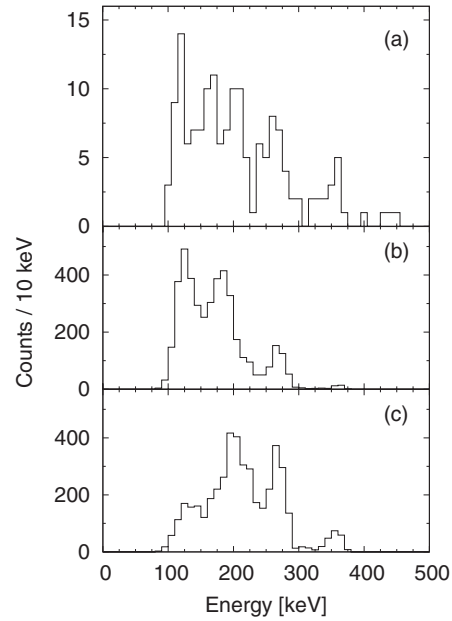

FIG. 4. (a) Energy spectrum of electrons detected in the DSSD temporally between the implantation of the ^{203}Fr recoil and the subsequent $9/2^-$ ground-state α decay. A correlation time of 150 ms was used between the recoil implantation and the conversion electron. (b) Energy spectrum of electrons from a GEANT4 simulation performed based on our interpretation of a three-step deexcitation and (c) for comparison a two-step deexcitation. See text for details.

Eight events from the α decay of the $1/2^+$ state in ^{203}Fr to the $1/2^+$ state in the daughter nucleus ^{199}At, with an α-particle energy of 7227(8) keV, have been reported by Uusitalo *et al.* [20]. Figure 3(a) presents the energy spectrum of the events from the α decay of the daughter astatine nuclei following the α decay of the parent francium nuclei in Fig. 1 with an energy of ~7240 keV. These events include the ones from the α decay of the $1/2^+$ isomer with the energy reported by Uusitalo *et al.* Three peaks are clearly visible, one of which represents the ground-state α decay of ^{199}At. The two other peaks originate from the α decays of ^{198}At following the α decays of the 3^+ ground state and the isomeric 10^- state, with the α-particle energies of 7241(8) keV and 7235(8) keV, respectively, in ^{202}Fr [20]. The half-life of the $1/2^+$ isomer was extracted by requiring the ground-state α decay of ^{199}At subsequent to the α decay of the isomer in ^{203}Fr. Using the maximum-likelihood method [40] for the time between the recoil implantation and the isomeric α decay, a half-life of 41^{+5}_{-4} ms was obtained. This value agrees well with the result of 60^{+30}_{-20} ms reported by Uusitalo *et al.* [20]. As the $1/2^+$ state in ^{203}Fr probably decays to the corresponding $1/2^+$ state in ^{199}At, and events from the $9/2^-$ ground-state α decay of ^{199}At are visible in Fig. 3(a), there must be an internal deexcitation branch depopulating the $1/2^+$ state in ^{199}At to the $9/2^-$ ground state. This branch will be discussed in detail later on in this section, but at this point it is justified to assume that there will be internal conversion contributing to the depopulation of the $1/2^+$ isomer to the $9/2^-$ ground state in ^{199}At, as the $1/2^+$ state will lie relatively low in energy. Figure 3(b) presents the energy spectrum of the events from the daughter α decays as in Fig. 3(a) but with a conversion electron required temporally between the two α decays in the same pixel of the DSSD. The events from the two decay chains of ^{202}Fr are filtered out, indicating that if there are any conversion electrons to be observed associated with the α decays of ^{202}Fr, they are below the detection threshold of the GREAT DSSD. Based on this observation, from the α decays in the peak consisting of events from ^{203}Fr and ^{202}Fr in Fig. 1, only the ones were chosen with a subsequent conversion electron observed. This α-electron pair gave a slight increase in statistics compared to using the α-α pair. From these events, an α-particle energy of 7246(5) keV was extracted for the decay of the $1/2^+$ state in ^{203}Fr.

Figure 4(a) presents the energy spectrum of the electrons detected in the DSSD, temporally between the implantation of the ^{203}Fr recoil and the subsequent $9/2^-$ ground-state α decay. The structure of the electron spectrum strongly resembles that obtained for the neighboring nucleus ^{205}Fr, associated with the depopulation of the $1/2^+$ isomer by an $M2$ transition to a $5/2^-$ state followed by a cascade consisting of two $M1$ transitions, one to a $7/2^-$ state followed by one to the $9/2^-$ ground state (see Ref. [15]). The FWHM is approximately 12 keV for the electron peaks in Fig. 4(a). Therefore the L- and higher-shell conversion electrons will not be separated, and a sum peak representing all these events should situate roughly 12–13 keV below the corresponding transition energy. In this special case, however, the internal conversion takes place inside the DSSD. Therefore, the energy deposited by the Auger electrons and low-energy x rays, released in the internal conversion process, sums up with the energy deposit of the conversion electron, giving an additional ~10 keV to the total energy deposit. As a result, the electron peak representing emission from the L + M (+ higher) shells is found close to

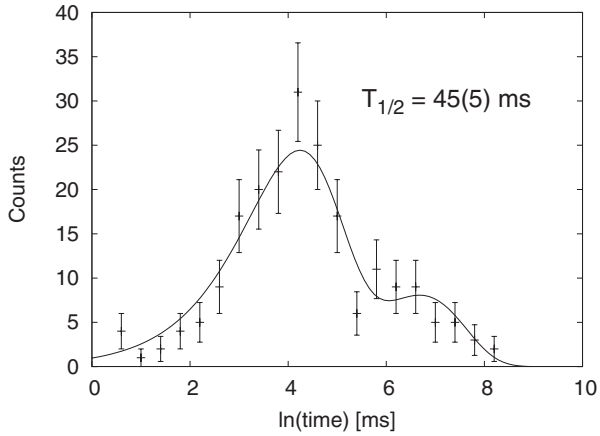

FIG. 5. Distribution of time differences between the implantation of the ^{203}Fr recoil in the DSSD and the subsequent electron detected in the same pixel before the $9/2^-$ ground-state α decay. Note the component consisting of random correlations on the right-hand side of the studied activity. See Ref. [48] for details on the method of using a logarithmic time scale.

2–3 keV below the corresponding transition energy. See our previous work on ^{205}Fr for a more detailed description on the analysis methods related to the electron spectra [15]. The distribution of time differences, see Fig. 5, obtained between the implantation of the ^{203}Fr recoil and the detection of the subsequent electrons, produces a half-life of 45(5) ms for the isomer. This value is in agreement with the value of 41^{+5}_{-4} ms obtained from the α-decay branch of the $1/2^+$ isomer, confirming that the electrons in Fig. 4(a) indeed originate from the branch that depopulates the $1/2^+$ isomer to the $9/2^-$ ground state. The half-life of the $1/2^+$ state is furthermore obtained as the weighted average 43(4) ms. Figure 6 presents the energy spectrum of γ rays detected with the GREAT clover and planar detector, and observed in coincidence with the electrons in Fig. 4(a). A 162-keV γ-ray peak is weakly visible alongside the francium x-ray peaks. Assuming this transition is, similarly as in ^{205}Fr, one of the $M1$ transitions, the structure

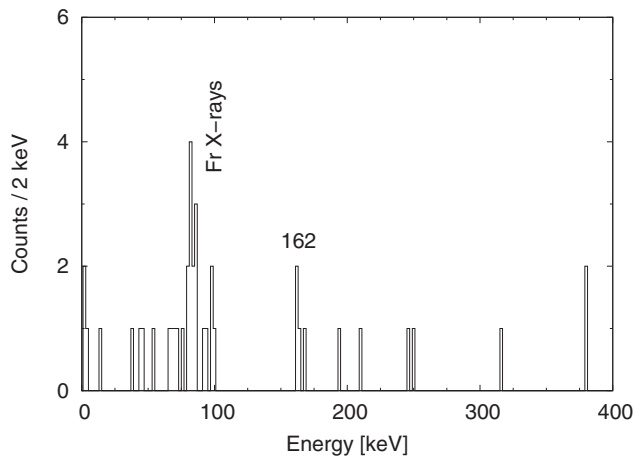

FIG. 6. Energy spectrum of γ rays detected with the GREAT clover detector and planar detector, and in coincidence with the electrons in Fig. 4(a).

of the electron spectrum can be explained as originating from a ∼20-keV $M2$ transition from the $1/2^+$ state followed by a cascade of a ∼175-keV $M1$ transition and the 162-keV transition. The 162-keV transition is visible in the prompt data and thus it is set to proceed to the $9/2^-$ ground state.

An energy spectrum of electrons, from the above-presented scenario, simulated using the GEANT4 package [41,42] is shown in Fig. 4(b). The similar shape of Fig. 4(b) and Fig. 4(a) supports our interpretation of the electron spectrum as representing a three-step cascade. To further confirm this interpretation, a simulation was made [see Fig. 4(c)], representing the alternative feasible scenario, where the $1/2^+$ isomer is depopulated solely by an $E3$ transition followed by the 162-keV transition to the $9/2^-$ ground state. Comparing the electron spectra from the two simulated scenarios with that in Fig. 4(a), it is likely that the electron spectrum in Fig. 4(a) actually results from the depopulation of the $1/2^+$ isomer being a combination of both scenarios. The fact that a γ-ray peak representing the ∼175-keV transition is not visible in Fig. 6 may additionally support the interpretation of a competing $E3$ transition depopulating the $1/2^+$ state to the $7/2^-$ state. Furthermore, while the 360-keV electron peak, representing the sum of the L + M + . . .-conversions of the transitions, is visible in all three spectra, it is less evident in Fig. 4(b). This could as well indicate the existence of a possible competing $E3$ branch in Fig. 4(a). Assuming a similar strength for this transition as in neighboring odd-mass nuclei [24,38,43] the $E3$ branch could be as high as 70%. Although the branching ratio cannot be determined to an acceptable precision due to low statistics, we suggest that the $E3$ branch is significant. Based on the α-particle and conversion-electron yields, a branching ratio of 20(4)% for the α decay of the $1/2^+$ isomer was obtained. Additionally, a reduced α-emission width of 51 keV was extracted for this decay using the method developed by Rasmussen [44], resulting in a hindrance factor of 1.1 as compared with the ground-state α decay of ^{202}Rn [45]. This is a sign of a favored α decay between states of equal spin and parity. Furthermore, a transition strength of $\sim 0.8 \times 10^{-4}$ W.u. was obtained for the ∼20-keV $M2$ transition assuming no competing $E3$ branch from the $1/2^+$ isomer. This result is in agreement with the strength of $3.5(2) \times 10^{-4}$ W.u. reported for the corresponding $M2$ transition in ^{205}Fr [15]. Moreover, the uncertainty of the branching ratio of the competing $E3$ transition does not affect the transition strength of the $M2$ transition to such an extent that it would create inconsistency with the assignment of an $M2$ multipolarity. Figure 7 presents a detailed view of the decay scheme. As the ∼175-keV γ-ray transition was not observed, the level energy of the $5/2^-$ state is set as tentative.

Figure 8(a) presents the energy spectrum of electrons following the α decay of the $1/2^+$ isomer of ^{203}Fr in the same DSSD pixel, and therefore representing the deexcitation of the $1/2^+$ state to the $9/2^-$ ground state in the daughter nucleus ^{199}At. The structure of the spectrum clearly differs from the one in Fig. 4(a) as there is a smaller number of peaks visible. Based on this observation, the assumption can be made that the depopulating cascade consists of less transitions than in ^{203}Fr, consisting for example of an $E3$ transition to a $7/2^-$ state followed by an $M1$ transition to the $9/2^-$ ground state.

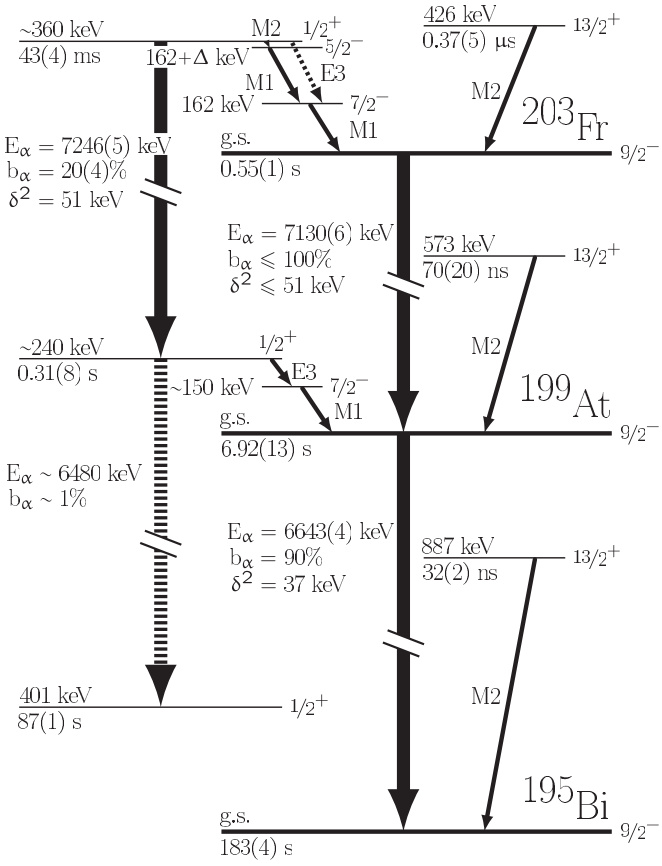

FIG. 7. The decay schemes of the $1/2^+$ state in ^{203}Fr and ^{199}At. For the ^{195}Bi data, see Refs. [51–53], for the ^{199}At data see the present work and Refs. [22,43,54] and for the ground-state α decay of ^{203}Fr see Refs. [20,36]. The α decay of the $1/2^+$ state in ^{199}At is presented with a dashed line as it has not been observed. $\Delta \sim 175$ keV, see text for details.

Figure 9 presents the distribution of time differences between the α decay of the $1/2^+$ state in ^{203}Fr and the subsequent electrons. A half-life of 0.31(8) s was obtained. Although no γ-ray transitions were seen in coincidence with the electrons in Fig. 8, both the astatine K- (four events) and L- (one event) x-ray peaks were observed with the GREAT clover and planar detector, indicating that one of the transitions in the cascade depopulating the $1/2^+$ isomer has to be above the energy threshold to produce a K-conversion electron. To understand the structure of the electron spectrum, the 150-keV peak may represent the L conversion of one of the two proposed transitions, and the 240-keV peak the sum of the L conversions of the two transitions. Based on these observations, the energy of the other transition would be ~90 keV. Furthermore, the intensity ratio of the two electron peaks in Fig. 8(a) supports our interpretation of the ~90-keV transition being of $E3$ character. Consequently, the ~150-keV transition would be of $M1$ character. Figure 8(b) presents an energy spectrum from a GEANT4 simulation of electrons from a cascade consisting of a 90-keV $E3$ and a 150-keV $M1$ transition. In Fig. 8(c) these transitions are in reversed order, i.e. a 150-keV $E3$ transition depopulating the $1/2^+$ isomer. Comparing the peak intensities in the two simulated spectra, it is evident that the

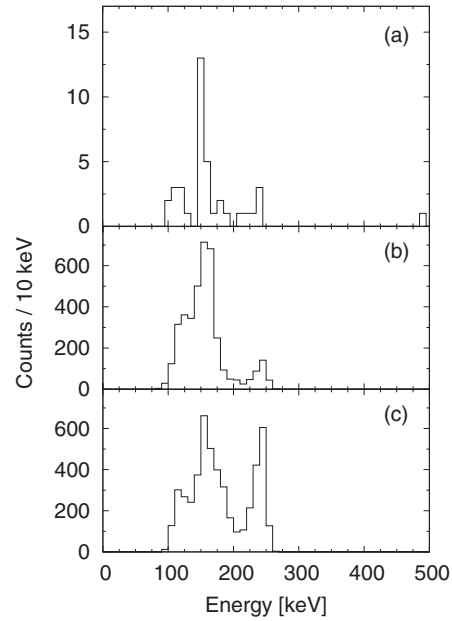

FIG. 8. (a) Energy spectrum of electrons detected in the DSSD following the α decay of the $1/2^+$ state in ^{203}Fr. A correlation time of 900 ms was used between the α decay and the subsequent electron. (b) Energy spectrum of electrons from a GEANT4 simulation performed based on our interpretation of a 90-keV $E3$ transition followed by a 150-keV $M1$ transition to the $9/2^-$ ground state. For comparison, an energy spectrum simulated for the reversed scenario, in which a 150-keV $E3$ transition is followed by a 90-keV $M1$ transition to the ground state, is shown in (c). See text for details.

results from the simulations support our interpretation of the cascade. A transition strength of ~0.09 W.u. was derived for the ~90-keV $E3$ transition, which is comparable with the strengths extracted for the corresponding transitions in ^{191}Bi and ^{195}At [24], respectively.

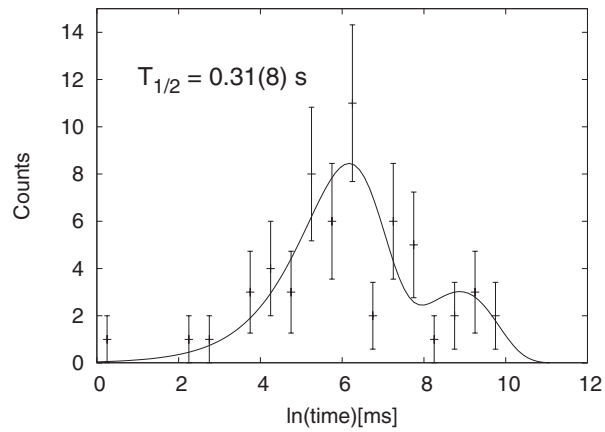

FIG. 9. Distribution of time differences between the α decay of the $1/2^+$ state in ^{203}Fr to the $1/2^+$ state in ^{199}At in the DSSD, and the subsequent electron detected in the same pixel. A maximum correlation time of 150 ms was used between the recoil implantation and the α decay. Note the component consisting of random correlations on the right-hand side of the studied activity. See Ref. [48] for details on the method of using a logarithmic time scale.

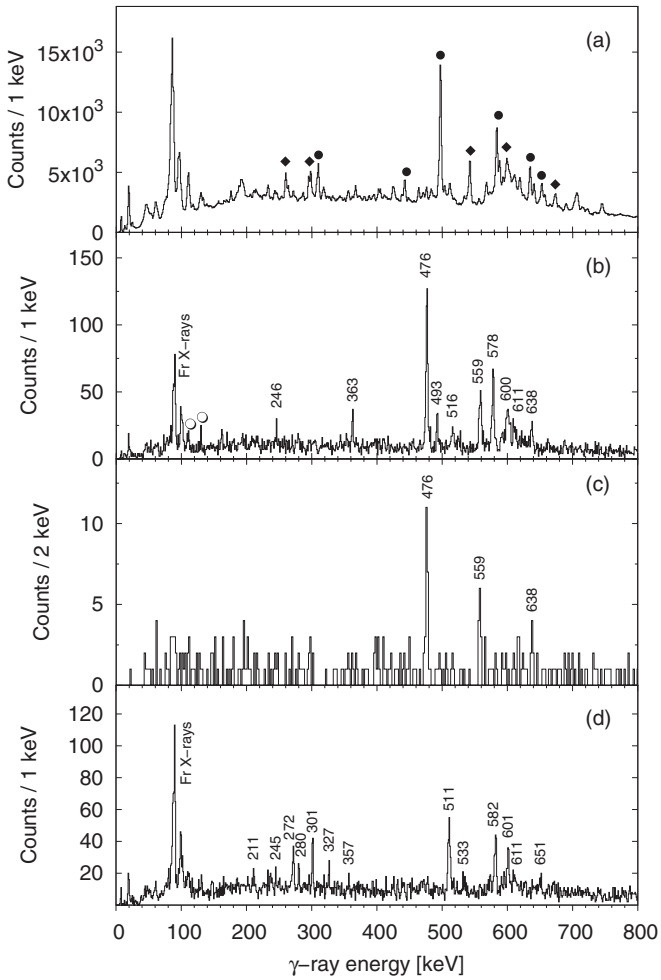

FIG. 10. Energy spectrum of prompt γ rays from the ^{40}Ar + ^{169}Tm reaction, detected with the JUROGAM array. (a) γ rays associated with any recoil detected in the GREAT DSSD. Peaks belonging to the dominant reaction channels ^{203}Rn and ^{204}Rn are marked with circles and diamonds, respectively. (b) γ rays tagged with the ^{203}Fr ground-state α decay. Peaks belonging to the contaminating ^{169}Tm [55] recoils are indicated by circles. (c) γ rays in the sum gate on the 476-, 559-, and 638-keV transitions. (d) γ rays associated with ^{204}Fr.

It is now worth noting that the level energies of the $1/2^+$ state in ^{203}Fr and ^{199}At fit well with the extracted α-particle energy from the decay of the $1/2^+$ state in ^{203}Fr, see Fig. 7. Additionally, by assuming a similar reduced width for the α decay of the $1/2^+$ state in ^{199}At as for the $9/2^-$ ground state, a branching ratio of $\sim$1% is predicted for the α decay. No events were observed from the α decay of the $1/2^+$ state in ^{199}At in the present data, as can be expected with such a low branching ratio combined with the low yield.

Figure 10(a) presents the energy spectrum of prompt γ rays detected with the JUROGAM array and associated with any fusion-evaporation recoil from the ^{40}Ar + ^{169}Tm reaction, detected in the GREAT DSSD. The strongest peaks belong to ^{203}Rn [46] and ^{204}Rn [9]. Prompt γ rays tagged with the ^{203}Fr ground-state α decay are presented in Fig. 10(b). The radon isotopes dominant in Fig. 10(a) are effectively filtered out. However, events from the Coulomb-excited ^{169}Tm target, indicated with open circles, still remain. The amount of statistics did only allow for a limited γ-γ coincidence analysis. However, three transitions with energies of 476-, 559-, and 638-keV were observed to be in coincidence. An energy spectrum of γ rays in coincidence with these three transitions is presented in Fig. 10(c). The transitions were sequenced according to the coincidence analysis and their intensities, with the 476-keV transition set as the lowest one, and each assigned an $E2$ multipolarity based on systematics in this region. The total population of the $13/2^+$ isomer was estimated by studying the yield of the depopulating $M2$ transition. This yield was then compared with the total intensity of the 476-keV transition. It was found that the total intensity of the 476-keV transition was too high for it to populate the $13/2^+$ state (and hence for the cascade to be built on top of this state) or the $1/2^+$ state. Therefore the cascade is assigned to be built on the $9/2^-$ ground state. Statistics did not allow for tagging with the electromagnetic transitions or α decays depopulating the $1/2^+$ or the $13/2^+$ isomers. The 246-, 363-, and 611-keV transitions are placed on the $13/2^+$ isomer based on intensity and energy sum relations, and in accordance with systematics. The 578-keV transition, prominent in Fig. 10(b) could not be associated with any of the other transitions in Fig. 10(b) and therefore remains unassigned. It could populate a higher-lying isomer or it could directly populate the $9/2^-$ ground state. The γ-ray transitions associated with ^{203}Fr [see Fig. 10(b)] are listed in Table I. See Fig. 11 for the level scheme.

α decays of the 3^+, 7^+, and 10^- states in ^{204}Fr [47] were observed in the experiment (see Fig. 1). The α-particle energies of 7013(5) keV and 7031(5) keV of the decays from the 10^- and 3^+ states, respectively, overlap, but the α-particle energy of 6969(5) keV from the decay of the 7^+ state is clearly distinguishable. The 10^- state is furthermore depopulated by a 275-keV $E3$ transition to the 7^+ state [15,47]. Using

TABLE I. The energies and relative intensities of prompt γ-ray transitions assigned to ^{203}Fr.

E_γ(keV)	I_γ(%)	I_i^π	I_f^π
161.9(4)	7(2)	$7/2^-$	$9/2^-$
245.5(4)[a]	7(2)	$(17/2^+)$	$(15/2^+)$
279.0(5)	6(2)		
344.2(6)	5(2)		
362.5(3)[a]	13(3)	$(15/2^+)$	$13/2^+$
367.8(3)	3(2)		
476.4(1)	100(6)	$13/2^-$	$9/2^-$
481.1(6)	7(3)		
492.5(3)	19(3)		
516.0(5)	13(4)		
558.6(2)	51(5)	$17/2^-$	$13/2^-$
578.1(2)	60(6)		
600.0(7)	24(9)		
603.5(9)	18(7)		
611.1(5)[a]	16(5)	$(17/2^+)$	$13/2^+$
637.7(3)[a]	18(4)	$(21/2^-)$	$17/2^-$

[a]The assignment of the γ-ray transition in the level scheme is tentative.

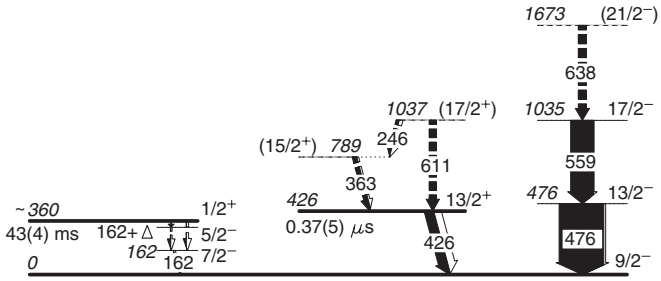

FIG. 11. The ^{203}Fr level scheme. Note that the intensities of the γ-ray transitions depopulating the $1/2^+$ isomer are not in scale. $\Delta \sim 175$ keV, see text and Fig. 7 for details. The black part of an arrow represents the γ-ray intensity of the transition and the white part the corresponding conversion-electron intensity.

the α decay of the 7^+ state for tagging, and requiring this 275-keV conversion electron temporally between the recoil implantation in the DSSD and the α decay in the same pixel, the half-lives of the 7^+ state and the 10^- state could be determined. By measuring the time differences between the conversion electron and the subsequent α decay a half-life of 2.6(3) s was obtained for the 7^+ state. This result is in full agreement with the half-life of 2.6(3) s reported by Huyse *et al.* [47]. Furthermore, by measuring the time differences between the recoil implantation and the subsequent conversion electron, a half-life of 1.65(15) s was obtained for the 10^- state. This result is slightly higher than that of approximately 1 s reported by Huyse *et al.* The method developed by Schmidt [48] was used to obtain the half-lives. Figure 10(d) presents the energy spectrum of prompt γ rays detected with the JUROGAM array and tagged with the α decays of the three states in ^{204}Fr. Statistics did not allow for an assignment of the transitions between the states.

IV. DISCUSSION

Both the $1/2^+$ state, based on a proton hole in the $s_{1/2}$ orbital, and the $13/2^+$ state, based on the odd proton in the $i_{13/2}$ orbital, are well known in the light odd-mass bismuth nuclei, see Fig. 12. The $13/2^+$ state lies quite constant in energy close to the $N = 126$ neutron shell closure, but comes down in energy when moving further toward the midshell. In the astatine nuclei the $13/2^+$ state is consistently lower in energy, but the down-sloping behavior is similar as in the bismuth nuclei. Furthermore, the state in the francium nuclei lies even lower in energy although no conclusions can yet be made of the systematics. In the astatine nuclei the proton-intruder $1/2^+$ state is only known in the lightest isotopes, and it becomes the ground state already in ^{195}At [19]. Based on systematics, it can be expected that the $1/2^+$ state becomes the ground state in ^{199}Fr as Uusitalo *et al.* [20] predict. The $7/2^-$ states observed in ^{203}Fr and ^{199}At are both suggested to originate from the odd proton in the $f_{7/2}$ orbital similarly as in ^{205}Fr [15]. This suggestion is reasonable, since the alternative $7/2^-$ state, originating from the $\pi h_{9/2} \otimes 2^+$ multiplet, should lie closer to the $13/2^-$ state. The level energy of the $5/2^-$ state remains tentative.

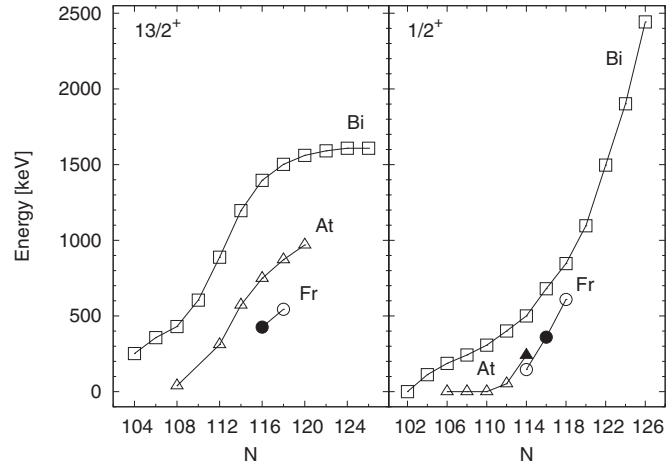

FIG. 12. Systematics of the $13/2^+$ state (left panel) and the $1/2^+$ state (right panel) in neutron-deficient odd-mass bismuth (squares), astatine (triangles), and francium (circles) nuclei. For the bismuth data see Refs. [16,56] and references therein, for the astatine data Refs. [18,19,21–23,39,49] and for the francium data Refs. [15,20]. ^{203}Fr has neutron number 116. The data points obtained from the present study are indicated with filled symbols.

The beginning of a possible rotational band was tentatively placed on top of the $13/2^+$ isomer. Comparing Fig. 10(b) with corresponding γ-ray spectra from neighboring odd-mass nuclei [15,22], it is evident that prominent γ-ray peaks, representing $M1$ transitions between the signature partners, a typical feature for a strongly coupled rotational band, are missing from Fig. 10(b). Furthermore, the intensity of the francium x-ray peaks relative to the intensity of the peak representing the γ-ray transition from the $13/2^-$ state to the $9/2^-$ ground state is significantly lower than in these neighboring odd-mass nuclei. The population of the $13/2^+$ state compared to the population of the ground state through the $13/2^-$ state state was estimated, and it is much lower in ^{203}Fr compared with these neighboring nuclei, see Table II. As the $13/2^+$ state becomes yrast in ^{203}Fr, it would be justified to expect that the population of this state would be relatively higher compared with the corresponding state in ^{205}Fr. Instead the population of the $13/2^+$ state is lower in ^{203}Fr than in ^{205}Fr. Furthermore, in ^{203}Fr the $13/2^+$ state is less populated in comparison with the ground-state population through the $13/2^-$ state. The most probable reason for this peculiarity is that there exists a higher-lying positive-parity

TABLE II. The population of the ground state through the $13/2^-$ state in ^{203}Fr and neighboring odd-mass nuclei as compared with the yield of the two γ-ray transitions populating directly the $13/2^+$ state. The number of ground-state α decays is used for normalization. The data are taken from our previous studies of the nuclei ^{197}At, ^{199}At [22], and ^{205}Fr [15].

Nucleus	^{197}At	^{199}At	^{203}Fr	^{205}Fr
$13/2^-$ vs g.s. α (%)	19 [a]	24 [a]	26	17
$13/2^+$ vs g.s. α (%)	26	28	10	24

[a]The yield of the $11/2^-$ state has been added.

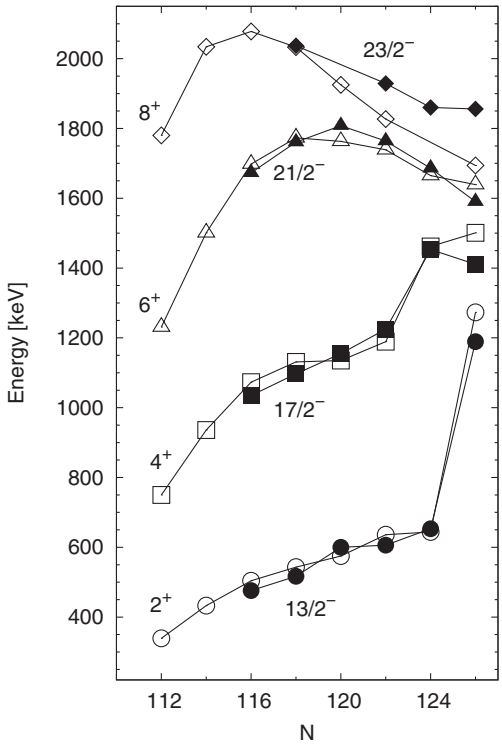

FIG. 13. Level energies of low-lying negative-parity states in neutron-deficient odd-mass francium nuclei (filled symbols) compared with yrast positive-parity states in their even-mass radon isotones (open symbols). ^{203}Fr has neutron number 116. For the radon data see Refs. [5,6,8–10]. The data for the heavier francium nuclei are taken from Refs. [12–15]. The lines connect yrast states without specifying the configuration of the states.

isomer feeding the negative-parity states via, e.g., an $E1$ transition. This isomer would be as fast as to decay inside RITU and none of the subsequent γ-ray transitions would be observed at the focal plane. A fast high-lying isomer has previously been observed in ^{209}Fr [13] with a spin and parity of $25/2^+$ ($\pi h_{9/2} \otimes \nu f_{5/2}^{-1} i_{13/2}^{-1}$) deexciting via an $E1$ transition to the $23/2^-$ ($\pi f_{7/2}$) state. This scenario could be the case in ^{203}Fr as well. Furthermore, similar fast $25/2^+$ isomers have been observed in light odd-mass astatine nuclei [21,49,50]. Such an isomer is not, however, reported in ^{205}Fr [15]. Unfortunately neither of the above-mentioned states have been observed in the present study, and therefore only speculations can be made concerning the curious weakness of the population of the $13/2^+$ state.

Figure 13 presents energy systematics of low-lying negative-parity states in neutron-deficient odd-mass francium nuclei compared with yrast positive-parity states in their radon isotones. The level energies of the states in ^{203}Fr fit well with systematics, showing an increase in collectivity when compared with the neighbor ^{205}Fr. No significant drops in the level energies, which would indicate an onset of ground-state deformation, can however yet be established. Based on these observations, the $13/2^-$, $17/2^-$, and $(21/2^-)$ states are assumed to originate from the odd $h_{9/2}$ proton coupled to the 2^+, 4^+, and 6^+ states, respectively, of the ^{202}Rn core.

V. CONCLUSION

The isomeric $13/2^+$ ($\pi i_{13/2}$) state was observed in ^{203}Fr. The beginning of a possible rotational band on top of this isomer was tentatively established, but a curious lack in population of the isomer was observed. There could, for example, be a high-lying positive-parity isomer feeding the negative-parity states instead of the $13/2^+$ state. The nature of this isomer could not be established. A ground-state feeding branch and the previously known α-decay branch from the deexcitation of the $1/2^+$ ($\pi s_{1/2}^{-1}$) state in ^{203}Fr were observed. The $1/2^+$ state in the α-decay daughter nucleus ^{199}At was observed as well. The level energies of this state both in ^{203}Fr and ^{199}At follow consistently the systematic behavior of the $1/2^+$ state observed in the odd-mass francium and astatine nuclei. A prompt γ-ray cascade was established on top of the the $9/2^-$ ground state. The structure of this cascade indicates that the dominance of the spherical structures in the ground state still prevails, as expected from the behavior of the neutron-deficient radon nuclei. Therefore the onset of oblate ground-state deformation is still pushed forward toward the neutron midshell. Continued studies toward the neutron midshell and ^{201}Fr could reveal interesting data as the ground state in ^{203}Fr is still spherical, while the ground state in ^{199}Fr is predicted to be oblate deformed. Moreover, a study, providing higher statistics than in the present work, is needed to further investigate the properties of the $13/2^+$ isomer in ^{203}Fr.

ACKNOWLEDGMENTS

This work has been supported through EURONS (European Commission Contract No. RII3-CT-2004-506065) and by the Academy of Finland under the Finnish Centre of Excellence Programme 2006-2011 (Nuclear and Accelerator Based Physics Contract No. 213503). The authors would also like to thank the UK/France (STFC/IN2P3) detector Loan Pool and GAMMAPOOL European Spectroscopy Resource for the loan of the detectors for the JUROGAM array. Support has also been provided by the UK Engineering and Physical Sciences Research Council. U.J. acknowledges support from the Finnish Academy of Science and Letters; Vilho, Yrjö, and Kalle Väisälä Foundation.

[1] R. Julin, K. Helariutta, and M. Muikku, J. Phys. G **27**, R109 (2001).
[2] A. M. Oros, K. Heyde, C. De Coster, B. Decroix, R. Wyss, B. R. Barrett, and P. Navratil, Nucl. Phys. A **645**, 107 (1999).
[3] K. Helariutta *et al.*, Eur. Phys. J. A **6**, 289 (1999).
[4] T. E. Cocolios *et al.*, Phys. Rev. Lett. **106**, 052503 (2011).
[5] G. D. Dracoulis, G. J. Lane, A. P. Byrne, P. M. Davidson, T. Kibédi, P. H. Nieminen, H. Watanabe, A. N. Wilson, H. L. Liu, and F. R. Xu, Phys. Rev. C **80**, 054320 (2009).

[6] A. R. Poletti, A. P. Byrne, G. D. Dracoulis, T. Kibédi, and P. M. Davidson, Nucl. Phys. A **756**, 83 (2005).
[7] W. J. Triggs, A. R. Poletti, G. D. Dracoulis, C. Fahlander, and A. P. Byrne, Nucl. Phys. A **395**, 274 (1983).
[8] D. Horn, C. Baktash, and C. J. Lister, Phys. Rev. C **24**, 2136 (1981).
[9] D. J. Dobson *et al.*, Phys. Rev. C **66**, 064321 (2002).
[10] R. B. E. Taylor *et al.*, Phys. Rev. C **59**, 673 (1999).
[11] H. Kettunen *et al.*, Phys. Rev. C **63**, 044315 (2001).
[12] A. P. Byrne, G. D. Dracoulis, C. Fahlander, H. Hübel, A. R. Poletti, A. E. Stuchbery, J. Gerl, R. F. Davie, and S. J. Poletti, Nucl. Phys. A **448**, 137 (1986).
[13] G. D. Dracoulis, P. M. Davidson, G. J. Lane, A. P. Byrne, T. Kibédi, P. Nieminen, H. Watanabe, and A. N. Wilson, Phys. Rev. C **79**, 054313 (2009).
[14] D. J. Hartley *et al.*, Phys. Rev. C **78**, 054319 (2008).
[15] U. Jakobsson *et al.*, Phys. Rev. C **85**, 014309 (2012).
[16] A. N. Andreyev *et al.*, Phys. Rev. C **69**, 054308 (2004).
[17] R. A. Braga, W. R. Western, J. L. Wood, R. W. Fink, R. Stone, C. R. Bingham, and L. L. Riedinger, Nucl. Phys. A **349**, 61 (1980).
[18] E. Coenen, K. Deneffe, M. Huyse, P. Van Duppen, and J. L. Wood, Z. Phys. A **324**, 485 (1986).
[19] H. Kettunen *et al.*, Eur. Phys. J. A **16**, 457 (2003).
[20] J. Uusitalo *et al.*, Phys. Rev. C **71**, 024306 (2005).
[21] K. Dybdal, T. Chapuran, D. B. Fossan, W. F. Piel, Jr., D. Horn, and E. K. Warburton, Phys. Rev. C **28**, 1171 (1983).
[22] U. Jakobsson *et al.*, Phys. Rev. C **82**, 044302 (2010).
[23] H. Kettunen *et al.*, Eur. Phys. J. A **17**, 537 (2003).
[24] M. Nyman *et al.* [Phys. Rev. C (to be published)].
[25] C. W. Beausang *et al.*, Nucl. Instrum. Methods Phys. Res. A **313**, 37 (1992).
[26] C. Rossi Alvarez, Nucl. Phys. News **3**, 10 (1993).
[27] M. Leino *et al.*, Nucl. Instrum. Methods Phys. Res. B **99**, 653 (1995).
[28] R. D. Page *et al.*, Nucl. Instrum. Methods Phys. Res. B **204**, 634 (2003).
[29] I. H. Lazarus *et al.*, IEEE Trans. Nucl. Sci. **48**, 567 (2001).
[30] K.-H. Schmidt *et al.*, Phys. Lett. B **168**, 39 (1986).
[31] R. S. Simon *et al.*, Z. Phys. A **325**, 197 (1986).
[32] E. S. Paul *et al.*, Phys. Rev. C **51**, 78 (1995).
[33] P. Rahkila, Nucl. Instrum. Methods Phys. Res. A **595**, 637 (2008).
[34] D. C. Radford, Nucl. Instrum. Methods Phys. Res. A **361**, 297 (1995).
[35] D. C. Radford, Nucl. Instrum. Methods Phys. Res. A **361**, 306 (1995).
[36] F. G. Kondev, Nucl. Data Sheets **105**, 1 (2005).
[37] T. Kibédi, T. W. Burrows, M. B. Trzhaskovskaya, P. M. Davidson, and C. W. Nestor, Jr., Nucl. Instrum. Methods Phys. Res. A **589**, 202 (2008).
[38] F. G. Kondev, Nucl. Data Sheets **108**, 365 (2007).
[39] K. Andgren *et al.*, Phys. Rev. C **78**, 044328 (2008).
[40] K.-H. Schmidt, C.-C. Sahm, K. Pielenz, and H.-G. Clerc, Z. Phys. A **316**, 19 (1984).
[41] S. Agostinelli *et al.*, Nucl. Instrum. Methods Phys. Res. A **506**, 250 (2003).
[42] J. Allison *et al.*, IEEE Trans. Nucl. Sci. **53**, 270 (2006).
[43] B. Singh, Nucl. Data Sheets **108**, 79 (2007).
[44] J. O. Rasmussen, Phys. Rev. **113**, 1593 (1959).
[45] S. Zhu and F. G. Kondev, Nucl. Data Sheets **109**, 699 (2008).
[46] H. Newman *et al.*, Phys. Rev. C **64**, 027304 (2001).
[47] M. Huyse, P. Decrock, P. Dendooven, G. Reusen, P. Van Duppen, and J. Wauters, Phys. Rev. C **46**, 1209 (1992).
[48] K.-H. Schmidt, Eur. Phys. J. A **8**, 141 (2000).
[49] R. F. Davie, A. R. Poletti, G. D. Dracoulis, A. P. Byrne, and C. Fahlander, Nucl. Phys. A **430**, 454 (1984).
[50] T. P. Sjoreen, U. Garg, and D. B. Fossan, Phys. Rev. C **23**, 272 (1981).
[51] Z. Chunmei, Nucl. Data Sheets **86**, 645 (1999).
[52] T. Lönnroth *et al.*, Phys. Rev. C **33**, 1641 (1986).
[53] H. Pai *et al.*, Phys. Rev. C **85**, 064317 (2012).
[54] H. De Witte *et al.*, Eur. Phys. J. A **23**, 243 (2005).
[55] C. M. Baglin, Nucl. Data Sheets **109**, 2033 (2008).
[56] P. Nieminen *et al.*, Phys. Rev. C **69**, 064326 (2004).